The Creation and Detection of Optical Modes with Spatial Light Modulators

Andrew Forbes[1,*], **Angela Dudley**[1,2] **and Melanie McLaren**[1]

[1]School of Physics,
University of the Witwatersrand, Private Bag 3, Wits 2050, South Africa

[2]CSIR National Laser Centre,
PO Box 395, Pretoria 0001, South Africa

[*]Corresponding author: andrew.forbes@wits.ac.za

Modal decomposition of light has been known for a long time, applied mostly to pattern recognition. With the commercialization of liquid crystal devices, digital holography as an enabling tool has become accessible to all, and with it all-digital tools for the decomposition of light has finally come of age. We review recent advances in unravelling the properties of light, from the modal structure of laser beams, to decoding the information stored in orbital angular momentum carrying fields. We show application of these tools to fibre lasers, solid-state lasers and structured light created in the laboratory by holographic laser beam shaping. We show by experimental implementation how digital holograms may be used to infer the intensity, phase, wavefront, Poynting vector, polarization and orbital angular momentum density of some unknown optical field. In particular, we outline how virtually all the previous ISO-standard beam diagnostic techniques may be readily replaced with all-digital equivalents, thus paving the way for unravelling of light in real-time. Such tools are highly relevant to the *in situ* analysis of laser systems, to mode division multiplexing as an emerging tool in optical communication, and for quantum information processing with entangled photons.
© 2015 Optical Society of America

OCIS codes: 090.1995, 070.6120, 140.3300, 140.3295, 120.3940, 060.2270, 030.4070

1. Introduction

There are many applications where the conventional mode from a laser will not suffice, for example, laser beams with a flat-top intensity structure are often more desirable for laser materials processing applications than those with a Gaussian intensity distribution [1]. Tailored light, structured light, complex light fields, laser beam shaping - these are

terms that are often used to describe the creation of customized light fields [2,3]. Many tools have been developed over the years to achieve this, ranging from refractive to diffractive, intra- and external to the laser cavity, passive and dynamic [4]. In parallel to the development of tools to create optical modes has been the development of tools to measure them. It was only in the early 1990s that standardized tools for characterizing laser beams were derived [5], mostly based on intensity measurements to infer, through propagation, the beam quality factor [6]. Later, wavefront sensors emerged as a real-time tool, but too expensive to become ubiquitous. Modally resolving the optical field, through a projective measurement with a match filter, was a known technique (often used in pattern recognition) but with a few exceptions [7] it was not applied to laser modes, again due to cost and complexity of the optical match filter.

More recently liquid crystal spatial light modulator technologies have emerged as an enabling tool for the on-demand creation of arbitrary optical fields. Such devices (see Fig. 1) have been extensively reviewed in the context of tutorials on getting started [8–10] as well as their various applications. The ease of use of such devices has spurned many new applications for real-time structured light, for example, holographic optical trapping and tweezing [11], quantum information processing [12], mode division multiplexling [13], microscopy [14], 3D holographic imaging and metrology [15–17] and even in lasers [18]. The same devices have been used to replicate and advance the previous static approaches. Today it is possible to create and detect optical modes with digital holograms, allowing for real-time rewritable tools that are inexpensive and easy to master.

Here we review the basic ideas for the creation and detection of optical modes with digital holograms written to spatial light modulators, showing how traditional techniques for the characterization of optical modes can be done with digital equivalents.

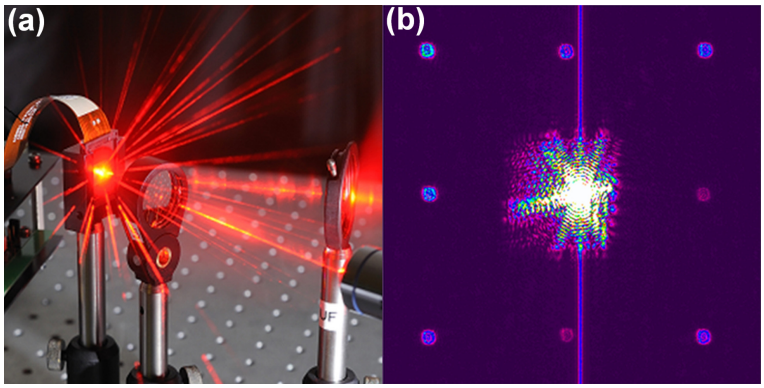

FIGURE 1. Liquid crystal spatial light modulators allow unprecedented control in the generation and detection of structured light fields. (a) Shows a long exposure image of laser light diffracted from the pixellated device. (b) A CCD camera image showing the various diffraction orders. Efficiencies are typically in the $60-85\%$ range.

2. Structured Light with Digital Holograms

We will begin with how to create and propagate optical modes using spatial light modulators, reviewing the current state of the art. In particular we review the known approaches for creating arbitrary optical modes by complex amplitude modulation on phase-only spatial light modulators, and provide some examples of the power of this technique. For more information on liquid crystal spatial light modulators the reader is referred to previous review and tutorial articles [8–10]. Consider the transformation of

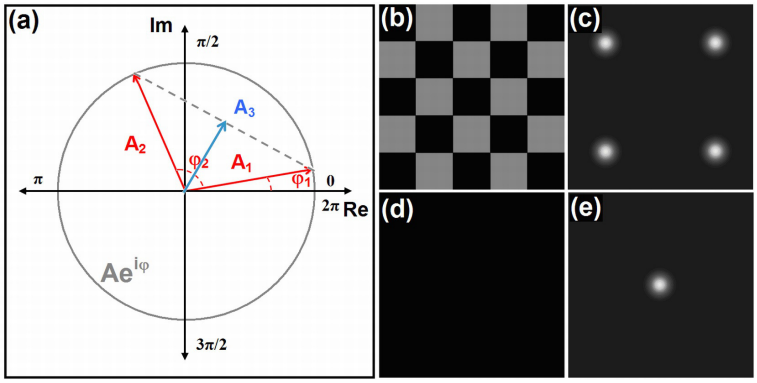

FIGURE 2. The so-called checker board approach for amplitude modulation on a phase-only spatial light modulator. A high carrier frequency is introduced across the device in the form of alternating phase values, with the resultant amplitude being the DC component. (a) Representation on the complex plane, (b) actual phase hologram for amplitude modulation, (c) the unwanted light is diffracted into higher orders which gives complete amplitude control over the desired order, e.g., from (d) zero transmission to (e) 100% transmission. Figure adapted with permission from [19].

an optical mode, $u_A = A_0 \exp(i\phi_A)$, of real-valued amplitude A_0 and real-valued phase ϕ_A, into a new mode $u_B = B_0 \exp(i\phi_B)$ in a single step through an optic with transmission function t. Then (with a few caveats):

$$u_B = t u_A \Rightarrow t = (B_0/A_0)\exp[i(\phi_B - \phi_A)]. \tag{1}$$

We see in this simple example that the transmission function requires both an amplitude and phase modulation. It is possible to encode this into optical elements and has for several decades now been possible with diffractive optical elements [20–23]. Such elements are rather difficult to fabricate and consequently such transformations have typically been executed in two steps with phase-only optics. In this approach, the first element creates the desired intensity pattern, leaving the phase as a free parameter, and the second element corrects the phase [4]. For this reason, many laser beam shaping solutions comprise two elements (one can think of a simple two-lens telescope in a similar fashion). This two-element approach can also be mimicked with phase-only spatial light modulators; the ease of implementing digital holograms on such devices has seen a resurgence in approaches to implement general complex amplitude modulation for the creation of arbitrary fields in a single step. The problem is to take the

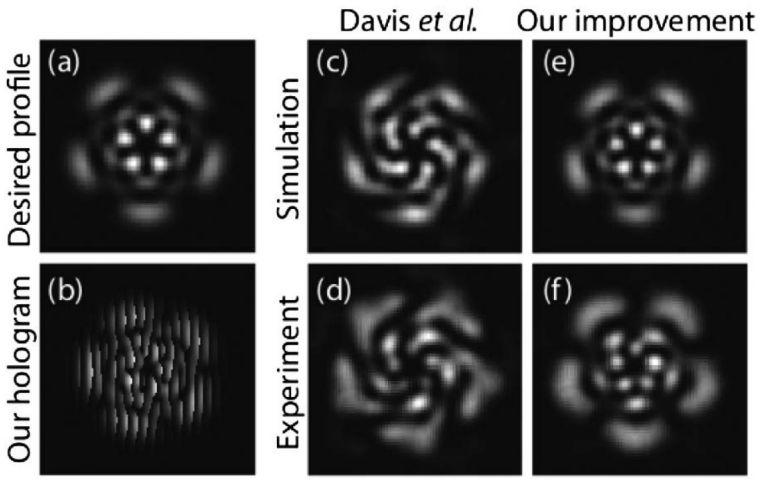

FIGURE 3. A comparison of two approaches for creating complex amplitude holograms on a phase-only device. The desired field (a) and its hologram (b) are encoded by the methods in refs [24] and [25], with the results shown in (c-d) and (e-f), respectively. Figure reprinted with permission from [25].

required transformation and convert it into a form that is phase-only, at least in some diffraction order:

$$t = (B_0/A_0)\exp[i(\phi_B - \phi_A)] \rightarrow \exp(i\Phi_{\text{slm}}). \tag{2}$$

Many techniques have been developed over the years to achieve this [24–36]. The core idea is to remove light from the first order in some spatially resolved manner. Since the device is phase-only, the light must go somewhere. As such, the techniques to do this can broadly be divided into two classes: (i) more light is directed to the zeroth order, or (ii) more light is directed to the higher diffraction orders. In the case of the former, the idea is simply to lower the diffraction efficiency spatially across the SLM by decreasing the depth of the phase step, while in the latter a high spatial frequency grating is added with a period that is spatially varying, so that more light is diffracted away from the first order. Both techniques rely on suitable filtering, usually at the Fourier plane after the SLM, to select the desired diffraction order. An example of this is shown in Fig. 2: a high spatial frequency in the form of a "checker board" diffracts light away from the first order. By filtering these orders out, the amplitude and phase of the desired order can be controlled. It has been shown that the quality of the created modes can be very high indeed [37–39], and that virtually any optical field can be created. The choice of approach depends largely on the problem being addressed, and results can vary if inappropriate encoding approaches are used (see example in Fig. 3). The creation of structured light fields by complex amplitude modulation has been applied and studied in the context of creating non-diffracting Bessel beams [19, 40–42], vortex beams carrying orbital angular momentum [43], vector beams [44–46] optical trapping and tweezing [11, 36, 47–49], quantum optics [50–52] and mode division multiplexing in free space and fibers (see for example [13] and references therein) to name but a

few. It is also possible to create these holograms in a wavelength independent manner: the phase transformation can be exact across a wide wavelength range albeit with some efficiency loss, opening the way to white light beam shaping with spatial light modulators [53]. Some examples of structured light fields and the associated holograms to create them are shown in Fig. 4. For example, in the creation of vortex beams that carry orbital angular momentum, either a phase-only hologram with a phase singularity can be encoded (part (a)) to produce an azimuthal phase, or complex amplitude modulation can be used (part (b)) to produce a Laguerre-Gaussian mode of the desired azimuthal order.

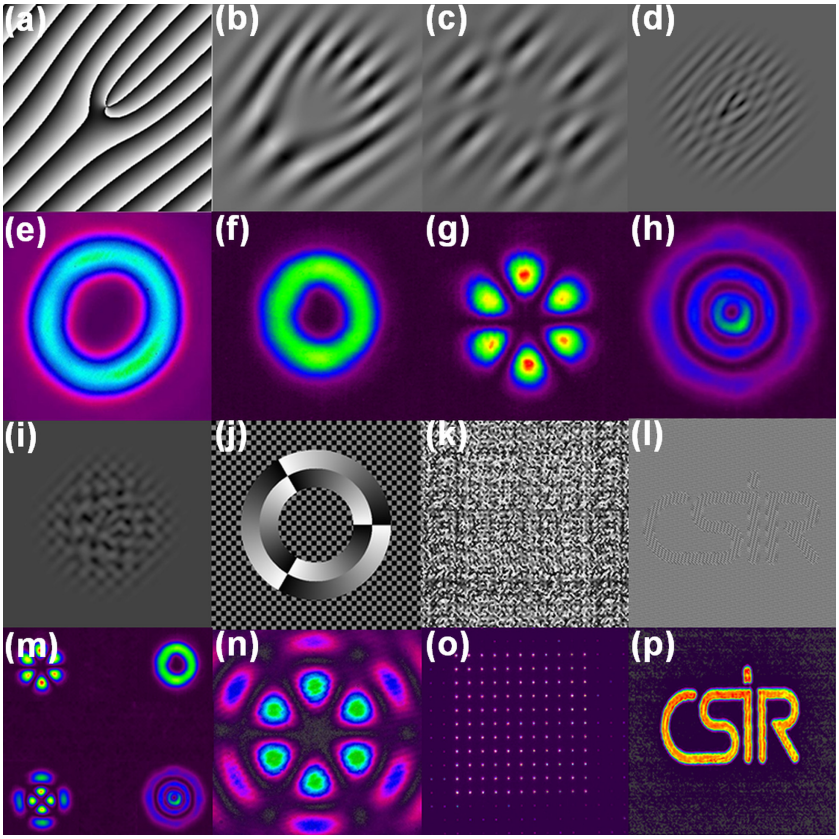

FIGURE 4. Examples of digital holograms employing various methods for the creation of structured light fields: (a) azimuthal phase-only; (b) Laguerre-Gaussian amplitude with azimuthal phase; (c) amplitude modulation to produce a superposition state of two azimuthal modes; (d) complex amplitude modulation for radial mode control; (i) multiplexed holograms to produce four modes or various radial and azimuthal indices; (j) azimuthal phase-only slits with a checkerboard to define the zero transmission regions; (k) hologram as a result of an iterative approach; (l) complex amplitude modulation to produce an arbitrary desired field. The experimental realization of each hologram is shown as the corresponding image below.

3. Digital Beam Diagnostics

Since the early 1990s a plethora of tools have been standardized for the measurement and characterization of laser beams based on statistical methods [5, 6, 54–58]. The core of the tools that are used in many laser laboratories on a daily basis involve time averaged measurements of the laser beam width, divergence and beam quality factor [59, 60]. Less common are measurements of the wavefront of the field [61].

A common tool for the measurement of a beam size is to scan a knife edge or aperture across the beam [54]; the integrated signal can be used to infer the beam width. If this is repeated as the beam propagates, at many points along the beam axis, then the divergence and beam quality factor (M^2) can be calculated by curve fitting routines. Today it is possible to replicate and in many instances improve on these methods by implementing them with digital holograms on spatial light modulators. One such demonstration was to perform an *in situ* tomography of a femtosecond optical beam with a holographic knife-edge [62]. In this example (see Fig. 5) the SLM was programmed with a time varying hologram that scanned a grating spatially across the field. The portion of the transmitted and deflected beam mimicked that of a knife-edge passing across the field. Because digital holograms are only gray-scale images, no moving parts were required for the measurement. This concept can be extended to other geometries that are not possible with mechanical devices, e.g., annular slits. Litvin *et. al* [63, 64] used the tools of complex amplitude modulation to create a hologram that allowed no light transmission except within a narrow annular ring-slit. Such slits have been used as static elements to create non-diffracting Bessel beams [65], but in this example the annular slit was scanned across the field in a radial direction, in an analogous manner to the lateral scanning of a knife-slit. The result was a measurement of the spatial intensity of the field with only a single point-like detector, i.e., without the need for a camera. Such concepts can be extended, for example, to create a digital variable pin-hole aperture.

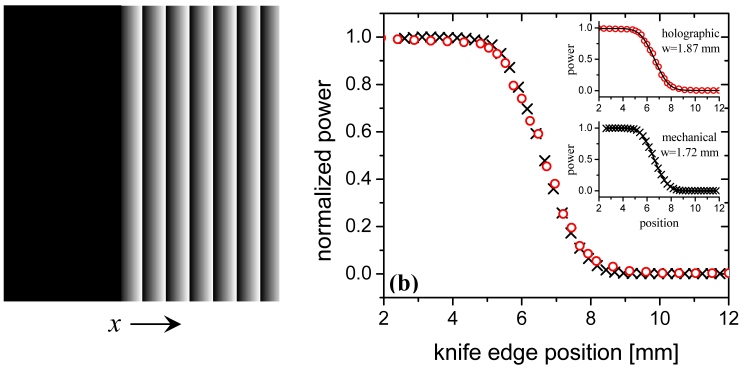

FIGURE 5. (a) A digital knife edge is scanned across the beam and the ratio of power in the zeroth and first diffraction orders monitored and plotted in (b). This is a digital equivalent to the ISO standard knife edge approach. Figure adapted with permission from [62].

Beam quality factor (M^2) measurements require that the beam size be measured as

a function of either a changing lens at a fixed distance, or a changing propagation distance with a fixed lens. Traditionally the latter is used as scanning the beam using a rail system is more convenient than cycling through a range of lenses. But with digital holograms, both are possible without any changes to the set-up other than a time varying digital hologram. Digital lenses can easily be programmed onto SLMs, and using this approach it has been shown that the beam quality factor of a laser beam can be measured with very high accuracy [66, 67]. To date this has been applied to the measurement of pure and superpositions of Laguerre-Gaussian modes with very good results, as shown in Fig. 6.

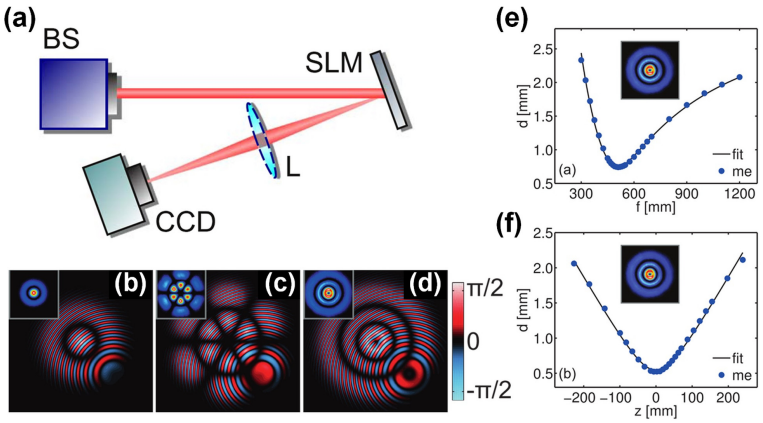

FIGURE 6. (a) Experimental approach to digitally propagate light, with all elements static. (b-d) Examples of holograms for mode creation and propagation. (e) and (f) show measured and calculated propagation data for Laguerre-Gaussian beams using the digital lens and digital propagation approaches, respectively. Figure adapted with permission from [67].

It is also possible to digitally propagate the field. It is well-known that numerical propagation of laser beams may be done with the aid of the angular spectrum of the light. It is intriguing to consider that if it can be done digitally on a computer, then it must be possible to do it digitally on an SLM too. Schulze *et al.* [67] showed that it is possible to simulate the propagation of any optical field using a time varying digital hologram and a static camera (see Fig. 6). In this work, they programmed the Fourier transform of the desired field and modulated it with the phase change of the plane waves due to propagation, $\exp(ik_z z)$, where k_z is the wavevector in the direction of propagation and z the propagation distance. By changing z in the hologram, the field appeared to propagate but with the observation at a single plane, i.e., the camera image showed the beam as if the camera was scanning along the z direction. The key here was to place the SLM in the back focal plane of the lens and observe the Fourier plane (front focal plane) with a camera. This tool allowed for fast, real-time measurement of the propagation of light, and has subsequently been applied to the propagation of accelerating light fields [68] and in novel imaging where the approach was used to digitally propagate to two different planes to observe two distinct images [69]. These tools have been combined with all-digital Stokes measurements on a spatial light modulator to demonstrate

wavefront and phase measurements of vector beams as they propagate [70].

4. Laser Beam Characterization by Modal Decomposition

The ISO standards for measuring laser beams also allow for a full modal decomposition to be performed. This idea dates back many decades to pattern recognition [71], and was later applied to optical modes with diffractive optical elements [7,72–74], in studies of Hermite-Gaussian modes [75], waveguides [76], solid-state laser systems [77], and fibers [78]. More recently it has been demonstrated with digital holograms written to spatial light modulators, circumventing the need for predetermined mode sets. In this section we outline the basic concept and highlight recent advances in the field using spatial light modulators.

The idea in modal decomposition is to take an unknown optical field and express it as a linear combination of basis functions, where it is convenient to select the basis functions from an orthogonal set of spatial modes:

$$u(\mathbf{r}) = \sum_{l=1}^{\infty} c_l \psi_l(\mathbf{r}), \tag{3}$$

with $\mathbf{r} = (x,y)$ the spatial coordinates, $c_l = \rho_l e^{i\varphi_l}$ the complex expansion coefficient with amplitude ρ_l and intermodal phase $\Delta\phi_l = \phi_l - \phi_0$. Now $\psi_l(\mathbf{r})$ represents one basis function; depending on the geometry of the problem, this would typically be a Hermite-Gaussian mode (rectangular symmetry), a Laguerre-Gaussian mode (circular symmetry) or perhaps an LP mode if fiber systems were under study. In fact, any orthogonal mode set will work and indeed have been used. It is clear that if the complex valued coefficients can be found from measurement (RHS of Eq. 3) then all the physical parameters of the unknown field (LHS of Eq. 3) can be inferred. The measurement of these coefficients is called modal decomposition: the unknown field is decomposed into modes with a particular weighting and phase between them. This is achieved by an inner product measurement of the field and each mode (individually) from the set: $\rho_l^2 = |<u|\psi_l>|^2$. Thus the inner product measurement yields an intensity in the Fourier plane (on axis) that is proportional to the power content of each mode (normalized so that $\sum_l \rho_l^2 = 1$). In general this operation can be performed using spatially multiplexed holograms so that many modes can be detected simultaneously. The hologram to perform this operation is often called a "match filter". An illustration of such inner product measurements is shown in Fig. 8.

To measure the intermodal phases with respect to a reference mode (usually assumed to be the zeroth mode), the inner product is performed twice to find

$$I_l^{\cos} = |<u(\mathbf{r})|(\psi_0(\mathbf{r}) + \psi_l(\mathbf{r}))>|^2, \tag{4}$$

$$I_l^{\sin} = |<u(\mathbf{r})|(\psi_0(\mathbf{r}) + i\psi_l(\mathbf{r}))>|^2, \tag{5}$$

from which we may find the intermodal phase $\Delta\phi_l$ without any ambiguity:

$$\Delta\phi_l = -\arctan\left[\frac{2I_l^{\sin} - \rho_l^2 - \rho_0^2}{2I_l^{\cos} - \rho_l^2 - \rho_0^2}\right]. \tag{6}$$

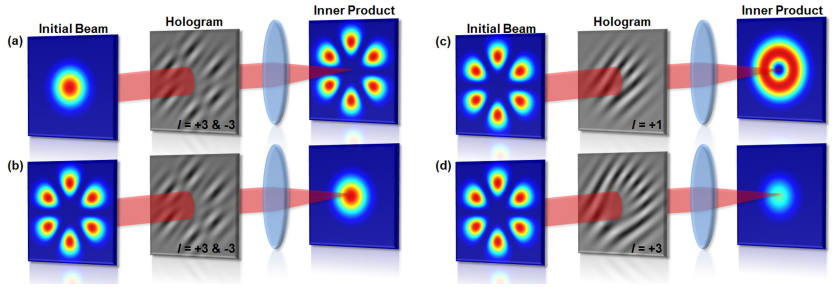

FIGURE 7. (a) When the incoming mode and the hologram do not "match", a central null is formed and no signal detected. (b) When the incoming mode and the hologram "match", i.e., they are complex conjugates of one another, then a central peak is formed and a signal detected. This is true for any combination of modes too, as illustrated in (c) and (d).

The main attraction of this approach over that of others is that with relatively few measurements, all the physical properties of an optical field can be inferred. It requires only point-like detectors and yet yields results with very high resolution (since the resolution is determined by the basis functions, which are not measured). This technique was implemented with spatial light modulators using the azimuthal modes, $\exp(i\ell\phi)$, as a basis set to study vortex beam lasers [80], and soon after to study fibers using the LP mode set [79] using a complete modal decomposition approach for full field reconstruction.

4.1. *Unravelling Optical Modes*

Modal decomposition with digital holograms has become a powerful tool to characterize laser beams because it offers high resolution results with only a few measurements. Moreover, any physical property of the field can be inferred once all the weighting coefficients are known, for example, amplitude, intensity, phase, wavefront, orbital angular momentum density, Poynting vector and so on. Many studies have employed the tool to do precisely this.

To illustrate the resolution issue as well as the power of the tool in determining both the wavefront and phase of light, several groups have studied holographic wavefront sensors as a means to reconstruct the wavefront and phase of scalar, vector, aberrated and vortex beams [81–84]. This is illustrated in Fig. 9, where the standard approach to wavefront and phase measurements using a Shack-Hartmann (SH) wavefront sensor was compared to the modal decomposition approach. In this study [81], with only three modal terms, the wavefront of the structured light beam was reconstructed with excellent fidelity and resolution, whereas the resolution of the SH wavefront sensor was limited (by the number of lenslets in the sampling array). Moreover, both the phase and the wavefront may be inferred from the modal decomposition, whereas the SHS can only measure wavefront (the two are often equal, but not always). This tool has been applied to vector and vortex beams [81], as well as to measure wavefront aberrations [82].

Modal decomposition has also been applied to the detection of modes carrying or-

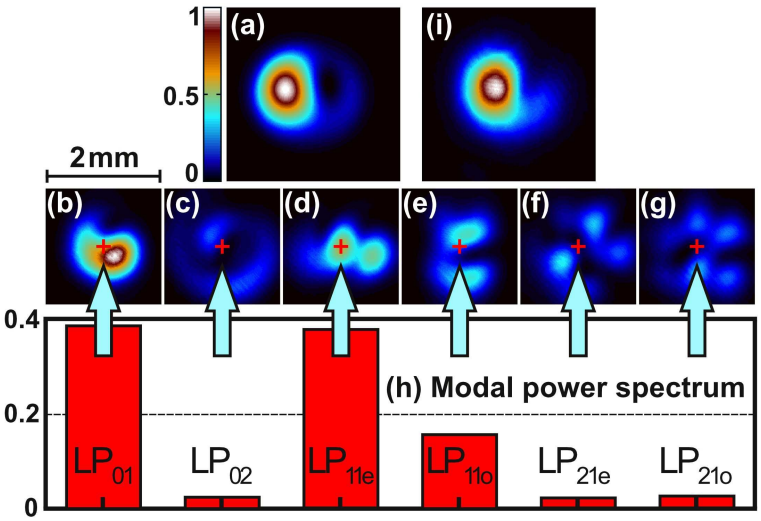

FIGURE 8. (a) Initial field (LHS of Eq. 3), (b)-(g) Actual measurements of the modal weights for each mode. The signal was detected at the position of the crosshairs. (h) Modal powers constructured from the measurements and finally (i) the reconstructed field using the modal approach (RHS of Eq. 3) . Figure reprinted with permission from [79].

bital angular momentum (OAM). Measuring OAM is a topic of intense study due to the myriad of opportunities it affords, e.g., in communications, optical traps and in quantum information processing. Techniques to measure OAM have been based on diffraction through apertures [85–87], interferometric sorting [88, 89], or optical transformation through refractive elements [90–92]. These techniques allow for the OAM mode to be detected but since no phase information is retrieved, the optical field cannot be reconstructed and the OAM density cannot be determined. It has been demonstrated that both the OAM and OAM density can be measured quantitatively [63, 93, 94] using the modal decomposition technique (see Fig. 10).

Despite the many advantages, there are some challenges. One issue that has attracted some attention is how to overcome the inherent yet unknown scale parameter of the mode set. For example, the Laguerre-Gaussian and Hermite-Gaussian modes have as an internal scale parameter the Gaussian beam size. The technique is known to work regardless of what value is selected here, but a poor choice has been shown to result in the requirement for many measurements, whereas the correct choice results in a minimum of measurements [95] (see Fig. 11). In the latter work it has been pointed out that while *any* basis and *any* scale will suffice, it possible to select an optimal value from one measurement without *a priori* of the scale [95], or to use a set of basis modes that have no scale, e.g., the azimuthal modes [64]. Doing so reduces the measurement terms and affords some ”reality” to the modal expansion (it is tempting to wish that the modes in the expansion are present in the beam and not mathematical constructs).

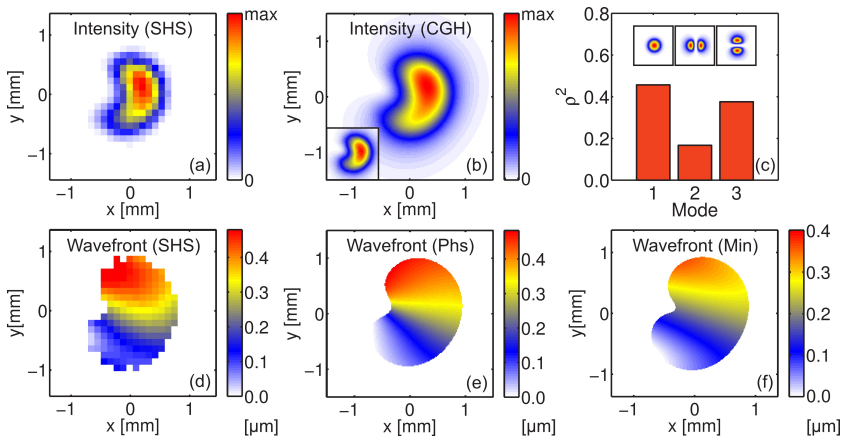

FIGURE 9. This example illustrates the power of the modal decomposition approach. Intensity and phase measurements using a Shack-Hartmann wavefront Sensor (SHS) are compared to reconstructed intensity and phase plots from a decomposition measurement of just three modes. The SHS results are pixelated whereas the modal results are not. Figure adapted with permission from [81].

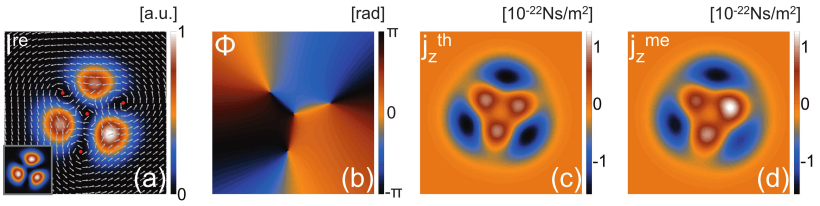

FIGURE 10. In this example the reconstructed intensity (a) and phase (b) are shown, along with the theoretical OAM density (c) together with the reconstructed plot using modal decomposition. Figure adapted with permission from [93].

4.2. *Application to Fibers*

An emerging research field is that of modal decomposition to monitor fibers. In one of the earliest works, computer generated match filters were used to measure the modal content of a graded-index fiber in terms of Laguerre-Gaussian mode [96], and then applied to study micro bends in such fibers [97]. Modal powers have subsequently been used to measure the output of fibers under ideal and non-ideal conditions, using the change in modal content as a performance monitor [79, 98, 99]. For example, as shown in Fig. 12, the bend loss of individual modes in a set-index fiber was successfully measured by modal decomposition - an important result for applications where fibers need to be bent (e.g., telecommunications). Such modal decomposition tools have been employed in a variety of fiber applications. In earlier work digital wavefront sensing (discussed earlier) has been applied to control the amplitude and phase of modes in a multimode fiber and to correct mode distortions [100, 101], while Flamm *et al.* used modal decomposition to optimize fiber-to-fiber coupling by monitoring the output modal spectrum [102]. Using the reconstruction properties of the modes, the beam quality factor

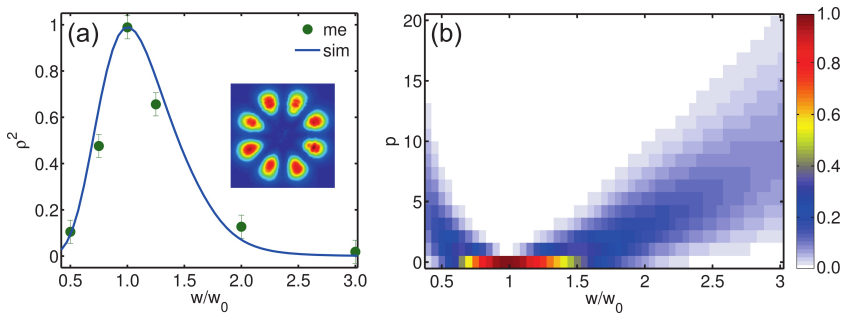

FIGURE 11. (a) When the scale in the Laguerre-Gaussian mode set is correctly chosen ($w = w_0$), then the decomposition requires only a single mode with all the power. (b) When the scale is not correctly chosen, more radial modes are required to describe this petal-like beam. As the assumed and actual scale difference increases, so more modes are required to correctly reconstruct the unknown field. Figure adapted with permission from [95].

and propagation characteristics of fiber output modes have been determined [103]. The approach has been extended to vector analysis to measure spatial polarization patterns of multimode beams from step-index fibers [104] and to measure the relative phases of vector modes in fibers [105]. In some cases the injected mode is also created by spatial light modulators offering a new tool for fiber analysis [99, 106–108].

Indeed, in mode division multiplexing applications, it is possible to both generate and detect the mode using spatial light modulators, e.g., [99, 109, 110]. Mode division multiplexing is a concept that dates back more than 30 years [111], but has gained attention recently due to the required bandwidth of present day optical communication systems [112], with seminal demonstrations in free space and fiber using spatial light modulators [113–117] (see for example, Fig. 14). While the focus is on fiber communications and LP modes, there has been significant interest in orbital angular momentum in both free space and fibers (see [13] and references therein), as well as customized mode-group sets [109] and multiplexing classical and quantum channels [118]. Vector modes in fibers are emerging as a new means by which to encode information where a combination of digital holograms and geometric phase elements are used in the detection scheme. There has been recent advances in this field in both free space [119, 120] and fibers [121]. Perturbations such as turbulence impact on performance of such links in free space, and spatial light modulators offer a means to study, characterize, and mitigate such effects [122, 123].

5. Modal Decomposition of Single Photons

The spatial modes of light hold promise for realizing high-dimensional quantum information processing and communication, going beyond the qubits (2 level systems) of polarization. The detection and manipulation of quantum states mirrors that of classical preparation and detection of structured light fields, and here we give a brief review of the progress made, at the single photon and quantum regime, in using digital holograms

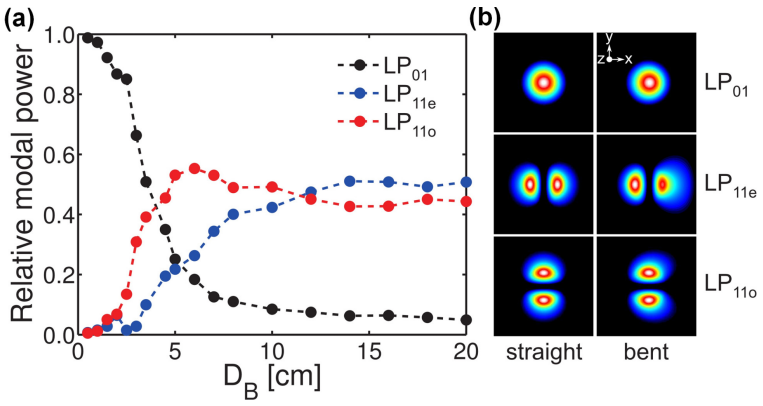

FIGURE 12. (a) Modal power changes as a function of the bending power (D_B) due to mode distortions in the bend versus straight fibre, as shown in (b). Figure reprinted with permission from [98].

as an enabling technology.

5.1. *Quantum State Tomography with Digital Holograms*

The early thought experiment by Einstein, Podolsky and Rosen (more commonly referred to as the EPR paradox) came to the conclusion that quantum mechanics was either an incomplete theory or involved non-local interactions [124]. Initial entanglement experiments used the orthogonal polarization states of photons to demonstrate the non-local nature of entangled particles [125–127]. In these early quantum experiments, polarizers were placed in each arm and rotated with respect to each other, such that a series of maxima and minima were recorded depending on the respective orientations of each polarizer. With the onset of spatial mode entanglement, polarization optics have been replaced with spatial light modulators to perform the equivalent measurements.

Quantum correlations measured in the orbital angular momentum (OAM) basis were first reported by Mair *et al*. [128] in 2001. Unlike the polarization states, OAM spans an infinite-dimensional Hilbert space and as such, an infinite amount of information can (theoretically) be encoded onto a photon. Using computer-generated holograms recorded onto holographic film, Mair *et al*. were able to show that, as with polarization or spin angular momentum, OAM is a property of single photons. In this experiment, static holograms were placed in the paths of both photons, collapsing the entangled quantum state into a single OAM state. When coupled to a single-mode fiber (SMF), this becomes an efficient method in which to measure the OAM of classical beams or single photons [129–131]. Only the fundamental mode (a Gaussian beam) can propagate through a SMF, such that the hologram together with the SMF, act as a ”match-filter”. The OAM spectrum or spiral bandwidth of the quantum state could then be elicited. This is comparable to the classical modal decomposition technique discussed earlier.

Of course, alternative methods to extract the OAM content have been demonstrated (see earlier discussion), however, it was in 2006 that the use of digital holograms were

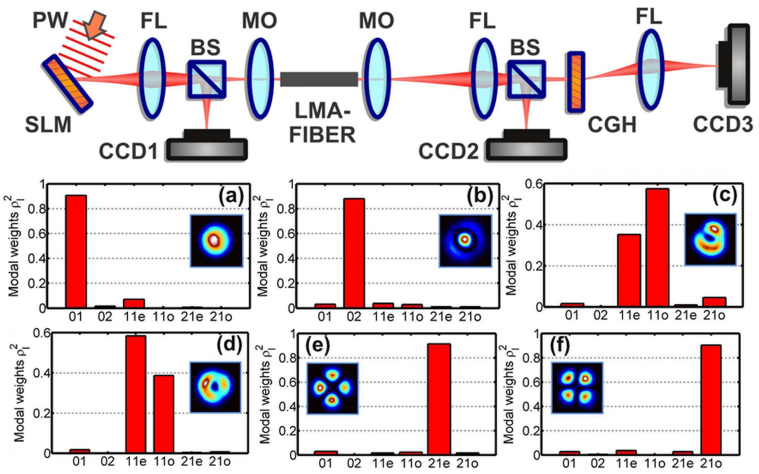

FIGURE 13. A toolbox for studying modal crosstalk in multimode fibers: a spatial light modulator is used to create the desired modes of the fiber, either individually or as superpositions. Modal decomposition is performed with a computer generated hologram (CGH), which can also be written to a spatial light modulator or encoded as a diffractive optical element. Modal analysis can be performed at both the input and output of the fiber. Figure reprinted with permission from [99].

first utilized to observe the entanglement of the spatial modes single photons [132]. Using phase-only spatial light modulators (SLMs), holograms were encoded with a helical phase term $\exp(i\ell\phi)$ together with a diffraction grating to produce the distinctive 'fork' holograms. There is a distinct advantage in using digital holograms as they can be varied without affecting the alignment of the entanglement setup [132–134]. Experiments requiring many different coincidence measurements can now be performed quickly and more accurately with sensitive digital alignment of holograms.

Quantum state tomography in particular requires a specific set of measurements using a variety of different holograms. The degree to which a quantum state is entangled can be determined by performing a full quantum state tomography to extract the density matrix [135]. This requires a set of measurements to be performed on identical copies of the quantum state, as any one measurement will affect the state. First proposed in 1957 [136], quantum tomography has become a well-established field [137–139]. Jack *et al.* first demonstrated this tomographic technique using digital holograms encoded onto SLMs, where the density matrix of a two-dimensional entangled state measured in the OAM basis was reconstructed [131]. The measurements required to reconstruct a density matrix consist of a set of both pure OAM modes as well as their superposition states, which can be represented by a Bloch sphere [140] (equivalent to the Poincaré sphere for polarization). In this experiment, Jack *et al.* chose a single two-dimensional OAM subspace and encoded both the two pure OAM states ($|\psi\rangle = \pm|\ell\rangle$) and four superposition states ($|\psi\rangle = |\ell\rangle + \exp(i\phi)|\ell\rangle$) onto each SLM. Projection measurements onto these six non-orthogonal states yielded a total of 36 coincidence measurements, from which the density matrix of the quantum state could be calculated. Technically,

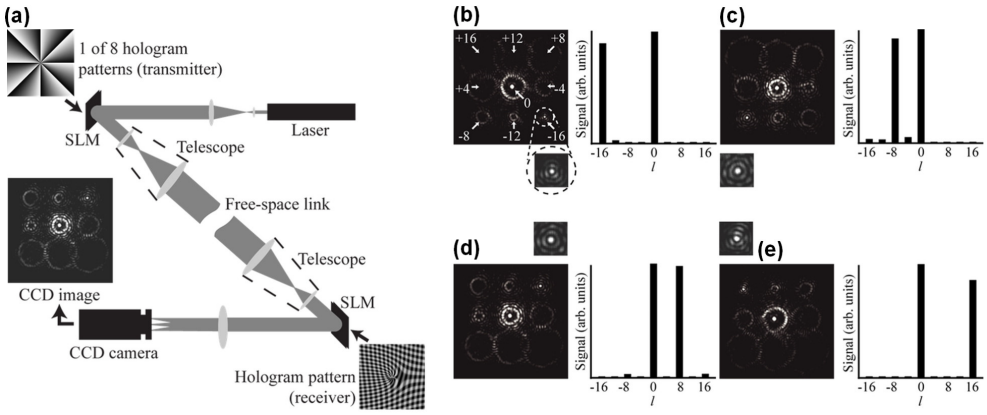

FIGURE 14. The first demonstration of multiplexing and demultiplexing OAM modes for free space communication. In this setup two SLMs are used: one for the mode creation and one for the mode detection, as shown in (a). Typical detector results and modal purity are shown in (b)-(e). Figure adapted with permission from [113].

a minimum of 16 measurements are required to reconstruct a two-dimensional density matrix, however with the versatility of digital holograms, the over-complete set of 36 measurements allows for a maximum-likelihood estimation to be made [137]. Additionally, the use of digital holograms in tomography is implemented in an automated system, where a set of measurements can be recorded without the need of continuous supervision.

This tomographic technique was then extended to measuring high-dimensional entangled states [142], where states were characterized up to dimension $d = 8$ by including additional OAM subspaces. With an increase in dimensionality, the number of required measurements also increases, where a total of 2025 coincidence measurements are required to reconstruct a 5-dimensional density matrix. By simply changing the projective measurement basis (by changing the encoded hologram) from the Laguerre-Gaussian (LG) to the Bessel-Gaussian (BG) basis, a widening of the measured OAM spectrum was observed. The BG modes include a continuous radial parameter (neglected in the LG case) and as such resulted in a relative increase in dimensionality [143]. When encoding both the azimuthal and radial components of the LG modes, amplitude modulation is required, which is significantly less efficient than the phase-only holograms, but also raises a number of difficulties. The accurate generation of LG modes with a non-zero radial index is a particular challenge [52, 144]. Various amplitude modulation techniques have been studied and achieved very high mode purities (see previous sections), however, in this modal decomposition technique, the beam coupled into the SMF must be a Gaussian and as such this term must be included when describing the overlap integral of the two-photon probability amplitude [52, 145]. This poses an issue as the phase function used to describe the full LG modes on the SLMs also contains a Gaussian term, which, if left untouched, results in a measurement of something other than the LG modes. It follows that the hologram must also include a

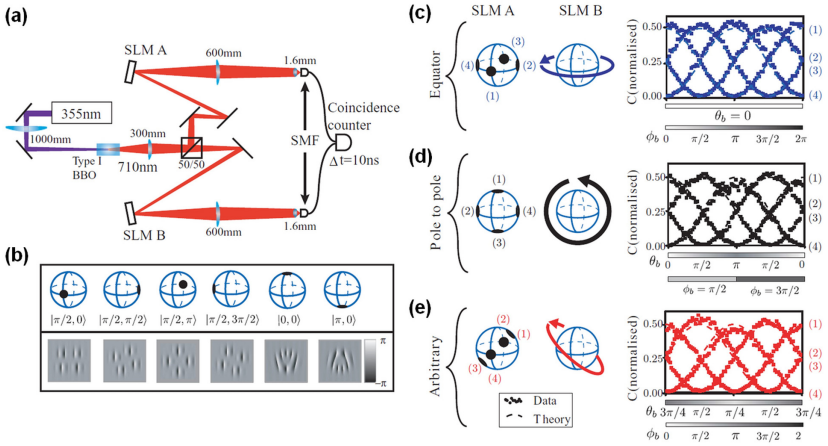

FIGURE 15. (a) Experimental setup showing the down-converted light from the crystal imaged onto the SLMs, and then reimaged at the plane of the single-mode fibers, where the detection and coincidence measurement takes place. (b) Typical phase masks - with appropriate intensity blazing - as would be displayed on an SLM. The two OAM eigenstates, Laguerre-Gauss, and four equally weighted superposition states, Hermite-Gauss, are shown). Bell curves for three different trajectories around (c) the equator, (d) poles, and (e) an arbitrarily chosen trajectory. Figure adapted with permission from [141].

term that acts to cancel the Gaussian term from the SMF. Despite the complications present with complex amplitude modulation, it has been shown that the inclusion of the radial components of the LG modes is crucial in correctly describing the amount of entanglement present in the spatial photon pairs [146].

Quantum state tomography has also been demonstrated using mutually unbiased bases (MUBs) [51, 147–149], where the simplest example of two-dimensional MUBs are the polarization states. Giovannini *et al.* were able to demonstrate high-dimensional entanglement up to dimension $d = 5$ and showed that the number of tomographic measurements required can be minimized using MUBs [149]. In this work, the OAM degree of freedom of single photons was used to define complete sets of MUBs, where one set of MUBs is represented by the pure OAM states and the other MUBs are the superposition states of the pure states [150]. The number of MUBs required to demonstrate d - dimensional entanglement is $(d + 1)$, such that a three-dimensional state would consist of four MUBs each with three different states. Each of the 12 states were encoded using complex amplitude modulation using the third technique found by Arrizón *et al.* [32].

5.2. Applications

The ability to digitally extract information from entangled photon pairs has been exploited not only in quantum tomography measurements, but extends into a variety of applications. Essential experimental measurements to test for quantum entanglement in the OAM basis have been successfully verified using the technique of digital modal

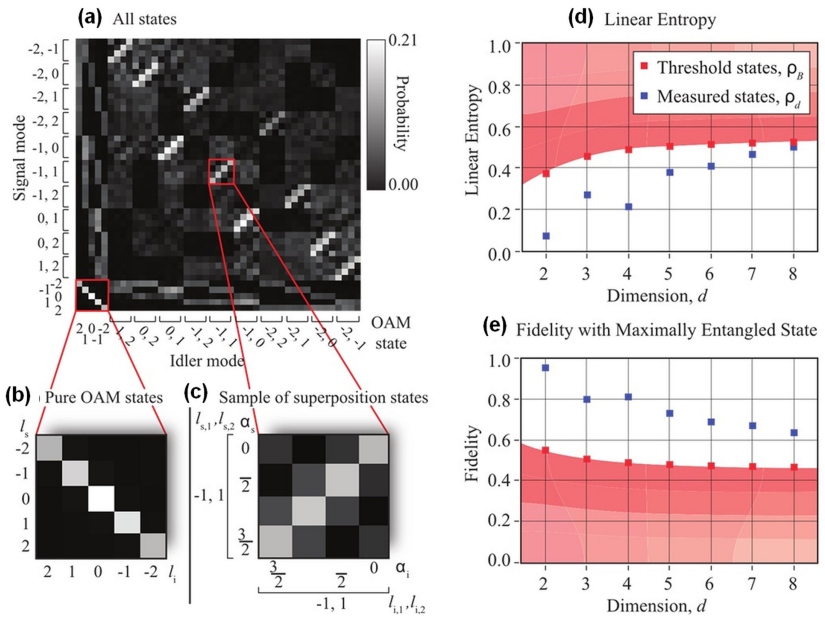

FIGURE 16. (a) The complete set of measured probabilities for dimension 5. (b) The pure OAM states. (c) A sample of the superposition states. Here, α_i denotes the phase difference in the idler arm, and α_s denotes the same in the signal arm. The OAM states separated by a comma denote ℓ_1, ℓ_2, while the single states denote ℓ. (d) Linear entropy and (e) fidelity as a function of dimension. The error for both of these measurements is ± 0.01, which is too small to be seen clearly on the graphs. In each case, the squares represent the measured data, while the circles represent the threshold states. The shaded area represents the set of states that will not violate the appropriate high-dimensional Bell inequality. Figure adapted with permission from [142].

decomposition. A violation of Bell's inequality, which distinguishes quantum correlations from classical ones, was demonstrated by Leach *et al.* in 2002 [88]. Similar to the experimental procedures undertaken using polarization, holograms encoded with a superposition state of a single OAM subspace, were rotated in each arm of the setup. The typical sinusoidal graph, predicted by theory [152], is also seen in the OAM basis, where the period of the maxima depends on the value of the OAM subspace. The same group then projected the entangled photons into the conjugate variable of OAM, angular position [153], and performed an EPR-type experiment highlighting the interesting entanglement between discrete (OAM) and continuous (angular position) variables [154]. Again, digital holograms were used to project the photons into a particular angular position. An aperture was encoded onto the existing fork-holograms to produce only a "slice " of the original hologram. The orientation of the holograms were varied with respect to each other, such that a maximum coincidence measurement was recorded when the orientations were identical. The width of the recorded spectrum depends directly on the width of the encoded slice-hologram.

This work led to the investigation into increasing the number of accessible OAM

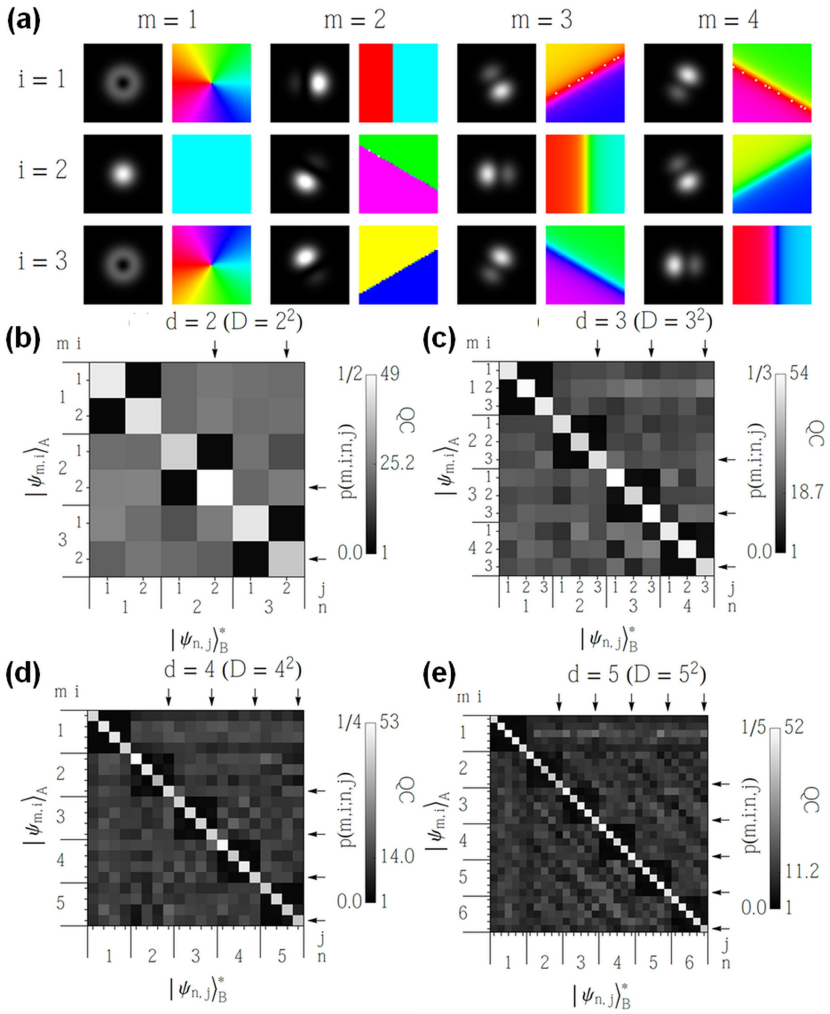

FIGURE 17. (a) The states for each of the four MUBs for $d = 3$. The theoretically calculated intensity profiles of the LG_ℓ are shown together with their corresponding measurement filters or holograms. (b-e)The normalized joint probabilities when SLM A (Alice) and SLM B (Bob) select one of the d states from one of the d + 1 bases for the entanglement-based scheme. Figure adapted with permission from [151].

states experimentally. A number of different groups explored various ways in which to increase the measured OAM spectrum [155–158]. One technique looks at the effect of the phase-matching of the non-linear crystal used to generate entangled photons and showed, by using particular "slit" holograms, that the spectrum can be increased by setting the crystal at a particular orientation [158].

Alternative methods to achieve high-dimensional entanglement have also been considered including a demonstration of entanglement up to dimension $d = 12$ through violations of Bell-type inequalities, where specific holograms were designed to project into measurement bases that maximize the violations of high-dimensional inequalities [159]. Exploiting other OAM-carrying modes, the Ince-Gaussian modes have also been shown to achieve high-dimensional entanglement for $d = 3$ by defining an entanglement witness for three dimensions [160]. And very recently, the same group experimentally verified 100-dimensional entanglement, projecting into both the azimuthal and radial components of the LG basis [161]. In each of these different techniques, the same modal transformation or decomposition was used to extract information from the entangled pairs.

Photons entangled in high dimensions present opportunities in applications such as quantum communication and cryptography, as each photon can be encoded with more information than those encoded in polarization. In quantum communication, high-dimensional entanglement offers increased information capacity per photon and the security is also improved, for example in quantum key distribution (QKD) in a noisy environment [162–165]. QKD allows two parties to share a secret key, which can then be used to encode and decode subsequent messages. The transmission of a quantum key has been securely performed using polarization states through fibers [166] as well as free space [167]. However, with digital holograms higher key generation rates have been achieved by increasing the dimensionality of the state using SLMs to project into high-dimensional MUBs [151]. In this case, digital holograms were used to encode both the phase and amplitude of the incident light to produce MUBs in the Laguerre-Gaussian basis.

In line with quantum communication, investigations into the effects of turbulence on entangled states have also made use of digital holography as an experimental technique [168–171]. Various theoretical works have examined the effects of atmospheric turbulence on OAM modes by considering the detection probability [172–174], attenuation and cross-talk among multiple OAM channels [175, 176]. Typically, the single phase screen approximation, which represents the turbulence according to the Kolmogorov theory [177], is used in theoretical simulations as well as experimental demonstrations. Experimentally, the turbulence is simulated by adding random phase fluctuations to the phase function (such as a fork-hologram) encoded onto the SLM. Using this technique, it was shown that higher OAM values are more robust through turbulence for both a single photon propagating through turbulence as well as both entangled photons experiencing turbulence [178].

6. Summary and Outlook

Laser beam shaping and characterization are venerable topics that experienced a resurgence at the birth of diffractive optics and computer generated holograms. Today, with the emergence of liquid crystal technology, structured light on-demand is achievable, and has found applications from the classical to the quantum. Despite the versatility of the technology, efficiency and power handling remain limitations which restrict industrial applications, whereas speed often prohibits real-time applications in the laboratory. As the technology matures, so one might expect more exciting advances to follow.

References

1. F. M. Dickey, T. E. Lizotte, S. C. Holswade, and D. L. Shealy, *Laser beam shaping applications* (CRC Press, 2005).
2. D. L. Andrews, *Structured light and its applications: An introduction to phase-structured beams and nanoscale optical forces* (Academic Press, 2011).
3. A. Forbes, *Laser beam propagation: generation and propagation of customized light* (CRC Press, 2014).
4. F. M. Dickey, *Laser beam shaping: theory and techniques* (CRC Press, 2014).
5. A. E. Siegman, "New developments in laser resonators," in "OE/LASE'90, 14-19 Jan., Los Angeles, CA," (International Society for Optics and Photonics, 1990), pp. 2–14.
6. A. E. Siegman, "Defining the effective radius of curvature for a nonideal optical beam," Quantum Electronics, IEEE Journal of **27**, 1146–1148 (1991).
7. V. A. Soifer and M. A. Golub, *Laser beam mode selection by computer generated holograms* (CRC Press, 1994).
8. B. Boruah, "Dynamic manipulation of a laser beam using a liquid crystal spatial light modulator," American Journal of Physics **77**, 331–336 (2009).
9. J. Pavlin, N. Vaupotič, and M. Čepič, "Liquid crystals: a new topic in physics for undergraduates," European Journal of Physics **34**, 745 (2013).
10. D. Huang, H. Timmers, A. Roberts, N. Shivaram, and A. S. Sandhu, "A low-cost spatial light modulator for use in undergraduate and graduate optics labs," American Journal of Physics **80**, 211–215 (2012).
11. M. Padgett and R. Bowman, "Tweezers with a twist," Nat. Photon. **5**, 343–348 (2011).
12. B. Jack, J. Leach, H. Ritsch, S. M. Barnett, M. J. Padgett, and S. Franke-Arnold, "Precise quantum tomography of photon pairs with entangled orbital angular momentum," New J. Phys. **11**, 103024 (2009).
13. A. Willner, H. Huang, Y. Yan, Y. Ren, N. Ahmed, G. Xie, C. Bao, L. Li, Y. Cao, Z. Zhao *et al.*, "Optical communications using orbital angular momentum beams," Advances in Optics and Photonics **7**, 66–106 (2015).
14. C. Maurer, A. Jesacher, S. Bernet, and M. Ritsch-Marte, "What spatial light modulators can do for optical microscopy," Laser & Photonics Reviews **5**, 81–101 (2011).
15. G. Nehmetallah and P. P. Banerjee, "Applications of digital and analog holography in three-dimensional imaging," Advances in Optics and Photonics **4**, 472–553 (2012).
16. W. Osten, A. Faridian, P. Gao, K. Körner, D. Naik, G. Pedrini, A. K. Singh, M. Takeda, and M. Wilke, "Recent advances in digital holography [invited]," Applied optics **53**, G44–G63 (2014).
17. P. Memmolo, L. Miccio, M. Paturzo, G. Di Caprio, G. Coppola, P. A. Netti, and P. Ferraro, "Recent advances in holographic 3d particle tracking," Advances in Optics and Photonics **7**, 713–755 (2015).
18. S. Ngcobo, I. Litvin, L. Burger, and A. Forbes, "A digital laser for on-demand laser modes," Nature communications **4** (2013).
19. A. Dudley, R. Vasilyeu, V. Belyi, N. Khilo, P. Ropot, and A. Forbes, "Controlling the evolution of nondiffracting speckle by complex amplitude modulation on a phase-only spatial light modulator," Opt. Commun. **285**, 5–12 (2012).

20. J. P. Kirk and A. L. Jones, "Phase-only complex-valued spatial filter," JOSA **61**, 1023–1028 (1971).
21. J. R. Izatt, "Checkerboard filters for gray-scale arrays," Appl. Optics **11**, 1407–1410 (1972).
22. Lee, "Binary synthetic holograms," Appl. Opt. **13**, 1677.
23. Lee, "Binary computer-generated holograms," Appl. Opt. **18**, 3661 (1979).
24. J. A. Davis, K. O. Valadéz, and D. M. Cottrell, "Encoding amplitude and phase information onto a binary phase-only spatial light modulator," Appl. Opt. **42**, 2003–2008 (2003).
25. E. Bolduc, N. Bent, E. Santamato, E. Karimi, and R. W. Boyd, "Exact solution to simultaneous intensity and phase encryption with a single phase-only hologram," Opt. Lett. **38**, 3546 (2013).
26. R. W. Cohn and M. Liang, "Approximating fully complex spatial modulation with pseudorandom phase-only modulation," Appl. Opt. **33**, 4406–4415 (1994).
27. R. W. Cohn, "Pseudorandom encoding of complex-valued functions onto amplitude-coupled phase modulators," JOSA A **15**, 868–883 (1998).
28. J. A. Davis, D. M. Cottrell, J. Campos, M. J. Yzuel, and I. Moreno, "Encoding amplitude information onto phase-only filters," Appl. Opt. **38**, 5004–5013 (1999).
29. V. Arrizón, "Optimum on-axis computer-generated hologram encoded into low-resolution phase-modul ation devices," Opt. Lett. **28**, 2521–2523 (2003).
30. V. Arrizón, "Complex modulation with a twisted-nematic liquid-crystal spatial light modulator: double-pixel approach," Opt. Lett. **28**, 1359–1361 (2003).
31. V. Arrizón, G. Méndez, and D. Sánchez-de La-Llave, "Accurate encoding of arbitrary complex fields with amplitude-only liquid crystal spatial light modulators," Opt. Express **13**, 7913–7927 (2005).
32. V. Arrizon, U. Ruiz, R. Carrada, and L. a. González, "Pixelated phase computer holograms for the accurate encoding of scalar complex fields." Journal of the Optical Society of America. A, Optics, image science, and vision **24**, 3500–7 (2007).
33. D. W. K. Wong and G. Chen, "Redistribution of the zero order by the use of a phase checkerboard pattern in computer generated holograms," Appl. Opt. **47**, 602–610 (2008).
34. E. G. Van Putten, I. M. Vellekoop, and A. P. Mosk, "Spatial amplitude and phase modulation using commercial twisted nematic lcds," Appl. Opt. **47**, 2076–2081 (2008).
35. M. Agour, C. Falldorf, and C. Von Kopylow, "Digital pre-filtering approach to improve optically reconstructed wavefields in opto-electronic holography," Journal of Optics **12**, 055401 (2010).
36. A. Jesacher, C. Maurer, A. Schwaighofer, S. Bernet, and M. Ritsch-Marte, "Full phase and amplitude control of holographic optical tweezers with high efficiency," Optics express **16**, 4479–4486 (2008).
37. T. Ando, Y. Ohtake, N. Matsumoto, T. Inoue, and N. Fukuchi, "Mode purities of laguerregaussian beams generated via complex-amplitude modulation using phase-only spatial light modulators," Opt. Lett. **34**, 34 (2009).
38. J. B. Bentley, J. A. Davis, M. A. Bandres, and J. C. Gutiérrez-Vega, "Generation of helical ince-gaussian beams with a liquid-crystal display," Opt. Lett. **31**, 649–651 (2006).
39. Y. Ohtake, T. Ando, N. Fukuchi, N. Matsumoto, H. Ito, and T. Hara, "Universal generation of higher-order multiringed laguerre-gaussian beams by using a spatial light modulator," Opt. Lett. **32**, 1411–1413 (2007).
40. C. López-Mariscal and K. Helmerson, "Shaped nondiffracting beams," Opt. Lett. **35**, 1215–1217 (2010).
41. R. Vasilyeu, A. Dudley, N. Khilo, and A. Forbes, "Generating superpositions of higher–order bessel beams," Opt. Express **17**, 23389–23395 (2009).
42. R. Rop, A. Dudley, C. López-Mariscal, and A. Forbes, "Measuring the rotation rates of superpositions of higher-order bessel beams," J. Mod. Opt. **59**, 259–267 (2012).
43. A. S. Ostrovsky, C. Rickenstorff-Parrao, and V. Arrizón, "Generation of the perfect optical vortex using a liquid-crystal spatial light modulator," Opt. Lett. **38**, 534–536 (2013).
44. C. Maurer, A. Jesacher, S. Fürhapter, S. Bernet, and M. Ritsch-Marte, "Tailoring of arbitrary optical vector beams," New Journal of Physics **9**, 78 (2007).
45. A. Dudley, Y. Li, T. Mhlanga, M. Escuti, and A. Forbes, "Generating and measuring nondiffracting vector bessel beams," Opt. Lett. **38**, 3429–3432 (2013).
46. X.-L. Wang, J. Ding, W.-J. Ni, C.-S. Guo, and H.-T. Wang, "Generation of arbitrary vector beams with a spatial light modulator and a common path interferometric arrangement," Opt. Lett. **32**, 3549–3551 (2007).

47. M. Woerdemann, C. Alpmann, M. Esseling, and C. Denz, "Advanced optical trapping by complex beam shaping," Laser & Photonics Reviews **7**, 839–854 (2013).
48. M. P. MacDonald, L. Paterson, K. Volke-Sepulveda, J. Arlt, W. Sibbett, and K. Dholakia, "Creation and manipulation of three-dimensional optically trapped structures," Science **296**, 1101–1103 (2002).
49. R. Bowman, V. DAmbrosio, E. Rubino, O. Jedrkiewicz, P. D. Trapani, and M. Padgett, "Optimisation of a low cost slm for diffraction efficiency and ghost order suppression," Eur. Phys. J. Special Topics **199**, 149 (2011).
50. M. T. Gruneisen, W. A. Miller, R. C. Dymale, and A. M. Sweiti, "Holographic generation of complex fields with spatial light modulators: application to quantum key distribution," Appl. Opt. **47**, A32–A42 (2008).
51. G. Lima, L. Neves, R. Guzmán, E. S. Gómez, W. A. T. Nogueira, A. Delgado, A. Vargas, and C. Saavedra, "Experimental quantum tomography of photonic qudits via mutually unbiased basis," Opt. Express **19**, 3542–3552 (2011).
52. Y. Zhang, F. S. Roux, M. McLaren, and A. Forbes, "Radial modal dependence of the azimuthal spectrum after parametric down-conversion," Phys. Rev. A **89**, 043820 (2014).
53. D. Spangenberg, A. Dudley, P. H. Neethling, E. G. Rohwer, and A. Forbes, "White light wavefront control with a spatial light modulator," Opt. Express **22**, 13870–13879 (2014).
54. A. E. Siegman, M. Sasnett, and T. Johnston Jr, "Choice of clip levels for beam width measurements using knife-edge techniques," Quantum Electronics, IEEE Journal of **27**, 1098–1104 (1991).
55. A. Siegman, "Defining and measuring laser beam quality," in "Solid State Lasers," (Springer, 1993), pp. 13–28.
56. M. W. SASNETT, "Characterization of laser beams: The m2 model," Handbook of optical and laser scanning p. 1 (2004).
57. A. E. Siegman, "Laser beams and resonators: The 1960s," IEEE Journal of selected topics in quantum electronics **6**, 1380–1388 (2000).
58. A. E. Siegman, "Laser beams and resonators: Beyond the 1960s," IEEE Journal of selected topics in quantum electronics **6**, 1389–1399 (2000).
59. "Lasers and laser-related equipment test methods for laser beam widths, divergence angles and beam propagation ratios part 1: Stigmatic and simple astigmatic beams," (2004).
60. "Lasers and laser-related equipment test methods for laser beam widths, divergence angles and beam propagation ratios part 2: General astigmatic beams," (2004).
61. "Lasers and laser-related equipment test methods for determination of the shape of a laser beam wavefront," (2005).
62. J. Strohaber, G. Kaya, N. Kaya, N. Hart, A. A. Kolomenskii, G. G. Paulus, and H. A. Schuessler, "In situ tomography of femtosecond optical beams with a holographic knife-edge," Opt. Express **19**, 14321–14334 (2011).
63. I. A. Litvin, A. Dudley, and A. Forbes, "Poynting vector and orbital angular momentum density of superpositions of bessel beams," Opt. Express **19**, 16760–16771 (2011).
64. I. A. Litvin, A. Dudley, F. S. Roux, and A. Forbes, "Azimuthal decomposition with digital holograms," Opt. Express **20**, 10996–11004 (2012).
65. J. Durnin, J. J. Miceli Jr, and J. H. Eberly, "Diffraction-free beams," Phys. Rev. Lett. **58**, 1499–1501 (1987).
66. J. Pérez-Vizcaíno, O. Mendoza-Yero, R. Martínez-Cuenca, L. Martínez-León, E. Tajahuerce, and J. Lancis, "Free-motion beam propagation factor measurement by means of a liquid crystal spatial light modulator," Journal of Display Technology **8**, 539–545 (2012).
67. C. Schulze, D. Flamm, M. Duparré, and A. Forbes, "Beam-quality measurements using a spatial light modulator," Opt. Lett. **37**, 4687–4689 (2012).
68. C. Schulze, F. S. Roux, A. Dudley, R. Rop, M. Duparré, and A. Forbes, "Accelerated rotation with orbital angular momentum modes," Physical Review A **91**, 043821 (2015).
69. J. A. Davis, I. Moreno, D. M. Cottrell, C. A. Berg, C. L. Freeman, A. Carmona, and W. Debenham, "Experimental implementation of a virtual optical beam propagator system based on a fresnel diffraction algorithm," Optical Engineering **54**, 103101–103101 (2015).
70. A. Dudley, G. Milione, R. R. Alfano, and A. Forbes, "All-digital wavefront sensing for structured

light beams," Opt. Express **22**, 14031–14040 (2014).
71. J. W. Goodman, *Introduction to Fourier optics* (Roberts and Company Publishers, 2005).
72. M. R. Duparre, V. S. Pavelyev, B. Luedge, E.-B. Kley, V. A. Soifer, and R. M. Kowarschik, "Generation, superposition, and separation of gauss-hermite modes by means of does," in "Optoelectronics and High-Power Lasers & Applications," (International Society for Optics and Photonics, 1998), pp. 104–114.
73. M. R. Duparre, V. S. Pavelyev, V. A. Soifer, and B. Luedge, "Laser beam characterization by means of diffractive optical correlation filters," in "International Symposium on Optical Science and Technology," (International Society for Optics and Photonics, 2000), pp. 40–48.
74. T. Kaiser, D. Flamm, M. DuparrÚ *et al.*, "Complete modal decomposition for optical fibers using cgh-based correlation filters," Opt. Express **17**, 9347–9356 (2009).
75. F. Gori, M. Santarsiero, R. Borghi, and G. Guattari, "Intensity-based modal analysis of partially coherent beams with hermitegaussian modes," Opt. Lett. **23**, 989–991 (1998).
76. O. Shapira, A. F. Abouraddy, J. D. Joannopoulos, and Y. Fink, "Complete modal decomposition for optical waveguides," Phys. Rev. Lett. **94**, 143902 (2005).
77. M. Duparré, B. Lüdge, and S. Schröter, "On-line characterization of nd: Yag laser beams by means of modal decomposition using diffractive optical correlation filters," in "Optical Systems Design 2005," (International Society for Optics and Photonics, 2005), pp. 59622G–59622G.
78. D. Beom Soo Soh, J. Nilsson, S. Baek, C. Codemard, Y. Jeong, and V. Philippov, "Modal power decomposition of beam intensity profiles into linearly polarized modes of multimode optical fibers," JOSA A **21**, 1241–1250 (2004).
79. D. Flamm, D. Naidoo, C. Schulze, A. Forbes, and M. Duparré, "Mode analysis with a spatial light modulator as a correlation filter," Opt. Lett. **37**, 2478–2480 (2012).
80. D. Naidoo, K. Aït-Ameur, M. Brunel, and A. Forbes, "Intra-cavity generation of superpositions of laguerre–gaussian beams," Applied Physics B **106**, 683–690 (2012).
81. C. Schulze, D. Naidoo, D. Flamm, O. A. Schmidt, A. Forbes, and M. Duparré, "Wavefront reconstruction by modal decomposition," Opt. Express **20**, 19714–19725 (2012).
82. C. Schulze, A. Dudley, D. Flamm, M. Duparré, and A. Forbes, "Reconstruction of laser beam wavefronts based on mode analysis," Appl. Opt. **52**, 5312–5317 (2013).
83. L. Changhai, X. Fengjie, H. Shengyang, and J. Zongfu, "Performance analysis of multiplexed phase computer-generated hologram for modal wavefront sensing," Appl. Opt. **50**, 1631–1639 (2011).
84. G. P. Andersen, L. Dussan, F. Ghebremichael, and K. Chen, "Holographic wavefront sensor," Optical Engineering **48**, 085801–085801 (2009).
85. J. M. Hickmann, E. J. S. Fonseca, W. C. Soares, and S. Chávez-Cerda, "Unveiling a truncated optical lattice associated with a triangular aperture using lights orbital angular momentum," Phys. Rev. Lett. **105**, 053904 (2010).
86. A. Mourka, J. Baumgartl, C. Shanor, K. Dholakia, and E. M. Wright, "Visualization of the birth of an optical vortex using diffraction from a triangular aperture," Opt. Express **19**, 5760–5771 (2011).
87. M. Mazilu, A. Mourka, T. Vettenburg, E. M. Wright, and K. Dholakia, "Simultaneous determination of the constituent azimuthal and radial mode indices for light fields possessing orbital angular momentum," Appl. Phys. Lett. **100**, 231115 (2012).
88. J. Leach, M. J. Padgett, S. M. Barnett, S. Franke-Arnold, and J. Courtial, "Measuring the orbital angular momentum of a single photon," Phys. Rev. Lett. **88**, 257901 (2002).
89. A. Lavery, M. P. J.mand Dudley, A. Forbes, J. Courtial, and M. J. Padgett, "Robust interferometer for the routing of light beams carrying orbital angular momentum," New J. Phys. **13**, 093014 (2011).
90. G. C. G. Berkhout, M. P. J. Lavery, J. Courtial, M. W. Beijersbergen, and M. J. Padgett, "Efficient sorting of orbital angular momentum states of light," Phys. Rev. Lett. **105**, 153601 (2010).
91. M. P. J. Lavery, D. J. Robertson, A. Sponselli, J. Courtial, N. K. Steinhoff, G. A. Tyler, A. E. Willner, and M. J. Padgett, "Efficient measurement of an optical orbital-angular-momentum spectrum comprising more than 50 states," New Journal of Physics **15**, 013024 (2013).
92. A. Dudley, T. Mhlanga, M. Lavery, A. McDonald, F. S. Roux, M. Padgett, and A. Forbes, "Efficient sorting of bessel beams," Opt. Express **21**, 165–171 (2013).
93. C. Schulze, A. Dudley, D. Flamm, M. Duparré, and A. Forbes, "Measurement of the orbital angular momentum density of light by modal decomposition," New J. Phys. **15**, 073025 (2013).

94. A. Dudley, I. Litvin, and A. Forbes, "Quantitative measurement of the orbital angular momentum density of light," Appl. Optics **51**, 823–833 (2012).
95. C. Schulze, S. Ngcobo, M. Duparré, and A. Forbes, "Modal decomposition without a priori scale information," Opt. Express **20**, 27866–27873 (2012).
96. H. O. Bartelt, A. W. Lohmann, W. Freude, and G. K. Grau, "Mode analysis of optical fibres using computer-generated matched filters," Electronics Letters **19**, 247–249 (1983).
97. V. Garitchev, M. Golub, S. Karpeev, S. Krivoshlykov, N. Petrov, I. Sissakian, V. Soifer, W. Haubenreisser, J.-U. Jahn, and R. Willsch, "Experimental investigation of mode coupling in a multimode graded-index fiber caused by periodic microbends using computer-generated spatial filters," Optics communications **55**, 403–405 (1985).
98. C. Schulze, A. Lorenz, D. Flamm, A. Hartung, S. Schröter, H. Bartelt, and M. Duparré, "Mode resolved bend loss in few-mode optical fibers," Opt. Express **21**, 3170–3181 (2013).
99. D. Flamm, C. Schulze, D. Naidoo, S. Schröter, A. Forbes, and M. Duparré, "All-digital holographic tool for mode excitation and analysis in optical fibers," Journal of Lightwave Technology **31**, 1023–1032 (2013).
100. M. Paurisse, M. Hanna, F. Druon, P. Georges, C. Bellanger, A. Brignon, and J. Huignard, "Phase and amplitude control of a multimode lma fiber beam by use of digital holography," Opt. Express **17**, 13000–13008 (2009).
101. M. Paurisse, L. Lévèque, M. Hanna, F. Druon, and P. Georges, "Complete measurement of fiber modal content by wavefront analysis," Opt. Express **20**, 4074–4084 (2012).
102. D. Flamm, K. Hou, P. Gelszinnis, C. Schulze, S. Schröter, and M. Duparré, "Modal characterization of fiber-to-fiber coupling processes," Opt. Lett. **38**, 2128–2130 (2013).
103. D. Flamm, C. Schulze, R. Brüning, O. A. Schmidt, T. Kaiser, S. Schröter, and M. Duparré, "Fast m¡ sup¿ 2¡/sup¿ measurement for fiber beams based on modal analysis," Appl. Opt. **51**, 987–993 (2012).
104. D. Flamm, O. A. Schmidt, C. Schulze, J. Borchardt, T. Kaiser, S. Schröter, and M. Duparré, "Measuring the spatial polarization distribution of multimode beams emerging from passive step-index large-mode-area fibers," Opt. Lett. **35**, 3429–3431 (2010).
105. S. Golowich, N. Bozinovic, P. Kristensen, and S. Ramachandran, "Complex mode amplitude measurement for a six-mode optical fiber," Opt. Express **21**, 4931–4944 (2013).
106. F. Dubois, P. Emplit, and O. Hugon, "Selective mode excitation in graded-index multimode fiber by a computer-generated optical mask," Opt. Lett. **19**, 433–435 (1994).
107. V. R. Daria, P. John Rodrigo, and J. Glückstad, "Programmable complex field coupling to high-order guided modes of micro-structured fibres," Opt. Comm. **232**, 229–237 (2004).
108. G. Stepniak, L. Maksymiuk, and J. Siuzdak, "Binary-phase spatial light filters for mode-selective excitation of multimode fibers," Journal of lightwave technology **29**, 1980–1987 (2011).
109. J. Carpenter, B. C. Thomsen, and T. D. Wilkinson, "Degenerate mode-group division multiplexing," Journal of Lightwave Technology **30**, 3946–3952 (2012).
110. C. Koebele, M. Salsi, D. Sperti, P. Tran, P. Brindel, H. Mardoyan, S. Bigo, A. Boutin, F. Verluise, P. Sillard *et al.*, "Two mode transmission at 2x100gb/s, over 40km-long prototype few-mode fiber, using lcos-based programmable mode multiplexer and demultiplexer," Opt. Express **19**, 16593–16600 (2011).
111. S. Berdagué and P. Facq, "Mode division multiplexing in optical fibers," Appl. Opt. **21**, 1950–1955 (1982).
112. D. J. Richardson, J. M. Fini, and L. E. Nelson, "Space-division multiplexing in optical fibres," Nat. Photon. **7**, 354–362 (2013).
113. G. Gibson and M. J. Courtial, J. and. Padgett, "Free-space information transfer using light beams carrying orbital angular momentum," Opt. Express **12**, 5448–5456 (2004).
114. N. Bozinovic, Y. Yue, Y. Ren, M. Tur, P. Kristensen, H. Huang, A. E. Willner, and S. Ramachandran, "Terabit-scale orbital angular momentum mode division multiplexing in fibers," Science **340**, 1545–1548 (2013).
115. H. Huang, G. Xie, Y. Yan, N. Ahmed, Y. Ren, Y. Yue, D. Rogawski, M. J. Willner, B. I. Erkmen, K. M. Birnbaum *et al.*, "100 tbit/s free-space data link enabled by three-dimensional multiplexing of orbital angular momentum, polarization, and wavelength," Opt. Lett. **39**, 197–200 (2014).

116. J. Wang, J. Yang, I. M. Fazal, N. Ahmed, Y. Yan, H. Huang, Y. Ren, Y. Yue, S. Dolinar, M. Tur, and A. E. Willner, "Terabit free-space data transmission employing orbital angular momentum multiplexing," Nat. Photon. **6**, 488–496 (2012).
117. F. Poletti, N. V. Wheeler, M. N. Petrovich, N. Baddela, E. N. Fokoua, J. R. Hayes, D. R. Gray, Z. Li, R. Slavík, and D. J. Richardson, "Towards high-capacity fibre-optic communications at the speed of light in vacuum," Nat. Photon. **7**, 279–284 (2013).
118. J. Carpenter, C. Xiong, M. J. Collins, J. Li, T. F. Krauss, B. J. Eggleton, A. S. Clark, J. Schröder, A. R. Albrecht, Y. Wang *et al.*, "Mode multiplexed single-photon and classical channels in a few-mode fiber." Opt. Express **21**, 28794–28800 (2013).
119. G. Milione, M. P. Lavery, H. Huang, Y. Ren, G. Xie, T. A. Nguyen, E. Karimi, L. Marrucci, D. A. Nolan, R. R. Alfano *et al.*, "4$\times$ 20 gbit/s mode division multiplexing over free space using vector modes and a q-plate mode (de) multiplexer," Optics letters **40**, 1980–1983 (2015).
120. G. Milione, T. A. Nguyen, J. Leach, D. A. Nolan, and R. R. Alfano, "Using the nonseparability of vector beams to encode information for optical communication," Optics letters **40**, 4887–4890 (2015).
121. H. Huang, G. Milione, M. P. Lavery, G. Xie, Y. Ren, Y. Cao, N. Ahmed, T. A. Nguyen, D. A. Nolan, M.-J. Li *et al.*, "Mode division multiplexing using an orbital angular momentum mode sorter and mimo-dsp over a graded-index few-mode optical fibre," Scientific reports **5** (2015).
122. G. Xie, L. Li, Y. Ren, H. Huang, Y. Yan, N. Ahmed, Z. Zhao, M. P. Lavery, N. Ashrafi, S. Ashrafi *et al.*, "Performance metrics and design considerations for a free-space optical orbital-angular-momentum–multiplexed communication link," Optica **2**, 357–365 (2015).
123. Y. Ren, G. Xie, H. Huang, L. Li, N. Ahmed, Y. Yan, M. P. Lavery, R. Bock, M. Tur, M. A. Neifeld *et al.*, "Turbulence compensation of an orbital angular momentum and polarization-multiplexed link using a data-carrying beacon on a separate wavelength," Optics Letters **40**, 2249–2252 (2015).
124. A. Einstein, B. Podolsky, and N. Rosen, "Can quantum-mechanical description of physical reality be considered complete?" Physical review **47**, 777 (1935).
125. J. Bell, "On the problem of hidden variables in quantum mechanics," Rev. Mod. Phys. **38**, 447–452 (1966).
126. A. Aspect, P. Grangier, and G. Roger, "Experimental realization of einstein-podolsky-rosen-bohm gedankenexperiment: A new violation of bell's inequalities," Phys. Rev. Lett. **49**, 91–94 (1982).
127. Y. Shih and C. Alley, "New type of einstein-podolsky-rosen-bohm experiment using pairs of light quanta produced by optical parametric down conversion," Phys. Rev. Lett. **61**, 2921–2924 (1988).
128. A. Mair, A. Vaziri, G. Weihs, and A. Zeilinger, "Entanglement of the orbital angular momentum states of photons," Nature **412**, 313–316 (2001).
129. A. Vaziri, G. Weihs, and A. Zeilinger, "Experimental two-photon, three-dimensional entanglement for quantum communication," Phys. Rev. Lett. **89**, 240401 (2002).
130. G. Molina-Terriza, J. P. Torres, and L. Torner, "Twisted photons," Nature Physics **3**, 305–310 (2007).
131. B. Jack, J. Leach, H. Ritsch, S. M. Barnett, M. J. Padgett, and S. Franke-Arnold, "Precise quantum tomography of photon pairs with entangled orbital angular momentum," New Journal of Physics **11**, 103024 (2009).
132. E. Yao, S. Franke-Arnold, J. Courtial, M. J. Padgett, and S. M. Barnett, "Observation of quantum entanglement using spatial light modulators," Opt. Express **14**, 13089–13094 (2006).
133. M. Stütz, S. Gröblacher, T. Jennewein, and A. Zeilinger, "How to create and detect n-dimensional entangled photons with an active phase hologram," Applied physics letters **90**, 261114 (2007).
134. G. Lima, A. Vargas, L. Neves, R. Guzmán, and C. Saavedra, "Manipulating spatial qudit states with programmable optical devices," Optics express **17**, 10688–10696 (2009).
135. K. Banaszek, G. M. DAriano, M. G. A. Paris, and M. F. Sacchi, "Maximum-likelihood estimation of the density matrix," Phys. Rev. A **61**, 010304(R) (1999).
136. U. Fano, "Description of states in quantum mechanics by density matrix and operator techniques," Rev. Mod. Phys. **29**, 74 (1957).
137. D. F. V. James, P. G. Kwiat, W. J. Munro, and A. G. White, "Measurement of qubits," Phys. Rev. A **64**, 052312 (2001).
138. R. T. Thew, K. Nemoto, A. G. White, and W. J. Munro, "Qudit quantum-state tomography," Phys. Rev. A **66**, 012303 (2002).

139. M. D. de Burgh, N. K. Langford, A. C. Doherty, and A. Gilchrist, "Choice of measurement sets in qubit tomography," Physical Review A **78**, 052122 (2008).
140. M. J. Padgett and J. Courtial, "Poincare-sphere equivalent for light beams containing orbital angular momentum," Opt. Lett. **24**, 430–432 (1999).
141. B. Jack, A. Yao, J. Leach, J. Romero, S. Franke-Arnold, D. Ireland, S. Barnett, and M. Padgett, "Entanglement of arbitrary superpositions of modes within two-dimensional orbital angular momentum state spaces," Phys. Rev. A **81**, 43844 (2010).
142. M. Agnew, J. Leach, M. McLaren, F. S. Roux, and R. W. Boyd, "Tomography of the quantum state of photons entangled in high dimensions," Phys. Rev. A **84**, 062101 (2011).
143. M. McLaren, J. Romero, M. J. Padgett, F. S. Roux, and A. Forbes, "Two-photon optics of bessel-gaussian modes," Phys. Rev. A **88**, 033818 (2013).
144. E. Karimi, D. Giovannini, E. Bolduc, N. Bent, F. M. Miatto, M. J. Padgett, and R. W. Boyd, "Exploring the quantum nature of the radial degree of freedom of a photon via hong-ou-mandel interference," Phys. Rev. A **89**, 013829 (2014).
145. Y. Zhang, M. Mclaren, F. S. Roux, and A. Forbe, "Simulating quantum state engineering in spontaneous parametric down-conversion using classical light," Opt. Express **22**, 17039 (2014).
146. V. D. Salakhutdinov, E. R. Eliel, and W. Löffler, "Full-field quantum correlations of spatially entangled photons," Phys. Rev. Lett. **108**, 173604 (2012).
147. R. B. A. Adamson and A. M. Steinberg, "Improving quantum state estimation with mutually unbiased bases," Phys. Rev. Lett. **105**, 030406 (2010).
148. A. Fernández-Pérez, A. B. Klimov, and C. Saavedra, "Quantum process reconstruction based on mutually unbiased basis," Phys. Rev. A **83**, 052332 (2011).
149. D. Giovannini, J. Romero, J. Leach, A. Dudley, A. Forbes, and M. J. Padgett, "Characterization of high-dimensional entangled systems via mutually unbiased measurements," Phys. Rev. Lett. **110**, 143601 (2013).
150. C. Spengler, M. Huber, S. Brierley, T. Adaktylos, and B. C. Hiesmayr, "Entanglement detection via mutually unbiased bases," Physical Review A **86**, 022311 (2012).
151. M. Mafu, A. Dudley, S. Goyal, D. Giovannini, M. McLaren, M. J. Padgett, T. Konrad, N. Petruccione, F.and Lütkenhaus, and A. Forbes, "Higher-dimensional orbital-angular-momentum-based quantum key distribution with mutually unbiased bases," Phys. Rev. A **88**, 032305 (2013).
152. J. Clauser, M. Horne, A. Shimony, and R. Holt, "Proposed experiment to test local hidden-variable theories," Phys. Rev. Lett. **23**, 880–884 (1969).
153. E. Yao, S. Franke-Arnold, J. Courtial, S. Barnett, and M. Padgett, "Fourier relationship between angular position and optical orbital angular momentum," Opt. Express **14**, 9071–9076 (2006).
154. J. Leach, B. Jack, J. Romero, A. Jha, A. Yao, S. Franke-Arnold, D. Ireland, R. Boyd, S. Barnett, and M. Padgett, "Quantum correlations in optical angle–orbital angular momentum variables," Science **329**, 662–665 (2010).
155. J. P. Torres, A. Alexandrescu, and L. Torner, "Quantum spiral bandwidth of entangled two-photon states," Phys. Rev. A **68**, 050301 (2003).
156. H. D. L. Pires, H. C. B. Florijn, and M. P. van Exter, "Measurement of the spiral spectrum of entangled two-photon states," Phys. Rev. Lett. **104**, 020505 (2010).
157. J. B. Pors, S. S. R. Oemrawsingh, A. Aiello, M. P. van Exter, E. R. Eliel, G. W. ́ı Hooft, and J. P. Woerdman, "Shannon dimensionality of quantum channels and its application to photon entanglement," Phys. Rev. Lett. **101**, 120502 (2008).
158. S. F.-A. S. M. B. J Romero, D Giovannini and M. J. Padgett, "Increasing the dimension in high-dimensional two-photon orbital angular momentum entanglement," (2012).
159. A. C. Dada, J. Leach, G. S. Buller, M. J. Padgett, and E. Andersson, "Experimental high-dimensional two-photon entanglement and violations of generalized bell inequalities," Nature Physics **7**, 677–680 (2011).
160. M. Krenn, R. Fickler, M. Huber, R. Lapkiewicz, W. Plick, S. Ramelow, and A. Zeilinger, "Entangled singularity patterns of photons in ince-gauss modes," Phys. Rev. A **87**, 012326 (2013).
161. M. Krenn, M. Huber, R. Fickler, R. Lapkiewicz, S. Ramelow, and A. Zeilinger, "Generation and confirmation of a (100$\times$ 100)-dimensional entangled quantum system," Proceedings of the National Academy of Sciences **111**, 6243–6247 (2014).

162. H. Bechmann-Pasquinucci and A. Peres, "Quantum cryptography with 3-state systems," Phys. Rev. Lett. **85**, 3313–3316 (2000).
163. V. Scarani, H. Bechmann-Pasquinucci, N. J. Cerf, M. Dušek, N. Ltkenhaus, and M. Peev, "The security of practical quantum key distribution," Rev. Mod. Phys. **81**, 1301 (2009).
164. G. Vallone, V. DAmbrosio, A. Sponselli, S. Slussarenko, L. Marrucci, F. Sciarrino, and P. Villoresi, "Free-space quantum key distribution by rotation-invariant twisted photons," Physical review letters **113**, 060503 (2014).
165. M. Mirhosseini, O. S. Magaña-Loaiza, M. N. OSullivan, B. Rodenburg, M. Malik, M. P. Lavery, M. J. Padgett, D. J. Gauthier, and R. W. Boyd, "High-dimensional quantum cryptography with twisted light," New Journal of Physics **17**, 033033 (2015).
166. P. A. Hiskett, D. Rosenberg, C. Peterson, R. Hughes, S. Nam, A. Lita, A. Miller, and J. Nordholt, "Long-distance quantum key distribution in optical fibre," New Journal of Physics **8**, 193 (2006).
167. R. Ursin, F. Tiefenbacher, T. Schmitt-Manderbach, H. Weier, T. Scheidl, M. Lindenthal, B. Blauensteiner, T. Jennewein, J. Perigues, P. Trojek, B. Ömer, M. Fürst, M. Meyenburg, J. Rarity, Z. Sodnik, C. Barbieri, H. Weinfurter, and A. Zeilinger, "Entanglement-based quantum communication over 144 km," Nature Phys. **3**, 481–486 (2007).
168. B.-J. Pors, C. H. Monken, E. R. Eliel, and J. P. Woerdman, "Transport of orbital-angular-momentum entanglement through a turbulent atmosphere," Opt. Express **19**, 6671–6683 (2011).
169. M. Malik, M. OSullivan, B. Rodenburg, M. Mirhosseini, J. Leach, M. P. J. Lavery, M. J. Padgett, and R. W. Boyd, "Influence of atmospheric turbulence on optical communications using orbital angular momentum for encoding," Opt. Express **20**, 13195 (2012).
170. B. Rodenburg, M. P. J. Lavery, M. Malik, M. N. O'Sullivan, M. Mirhosseini, D. J. Robertson, M. Padgett, and R. W. Boyd, "Influence of atmospheric turbulence on states of light carrying orbital angular momentum," Opt. Lett. **37**, 3735 (2012).
171. M. Krenn, R. Fickler, M. Fink, J. Handsteiner, M. Malik, T. Scheidl, R. Ursin, and A. Zeilinger, "Communication with spatially modulated light through turbulent air across vienna," New Journal of Physics **16**, 113028 (2014).
172. C. Paterson, "Atmospheric turbulence and orbital angular momentum of single photons for optical communication," Phys. Rev. Lett. **94**, 153901 (2005).
173. C. Gopaul and R. Andrews, "The effect of atmospheric turbulence on entangled orbital angular momentum states," New J. Phys. **9**, 94 (2007).
174. G. A. Tyler and R. W. Boyd, "Influence of atmospheric turbulence on the propagation of quantum states of light carrying orbital angular momentum," Opt. Lett. **34**, 142–144 (2009).
175. B. J. Smith and M. G. Raymer, "Two-photon wave mechanics," Phys. Rev. A **74**, 062104 (2006).
176. F. S. Roux, "Infinitesimal-propagation equation for decoherence of an orbital-angular-momentum-entangled biphoton state in atmospheric turbulence," Phys. Rev. A **83**, 053822 (2011).
177. L. C. Andrews and R. L. Phillips, *Laser Beam Propagation Through Random Media* (SPIE, Washington, 1998).
178. A. Hamadou Ibrahim, F. S. Roux, M. McLaren, T. Konrad, and A. Forbes, "Orbital-angular-momentum entanglement in turbulence," Phys. Rev. A **88**, 012312 (2013).